Multibody Syst Dyn (2010) 23: 431–451
DOI 10.1007/s11044-009-9186-y

Human lifting simulation using a multi-objective optimization approach

Yujiang Xiang · Jasbir S. Arora · Salam Rahmatalla · Timothy Marler · Rajankumar Bhatt · Karim Abdel-Malek

Received: 21 April 2009 / Accepted: 29 December 2009 / Published online: 21 January 2010

Abstract This paper presents a multiobjective optimization (MOO) approach to predicting dynamic lifting for a three-dimensional, highly redundant digital human model with 55 degrees of freedom. The optimization problem is formulated to optimize two objective functions simultaneously—dynamic effort and stability—subject to basic physical and kinematical constraints. The predictive dynamics approach is used to solve for the joint angles, torque profiles, and ground reaction forces. The weighted sum approach of MOO is used to aggregate the two objective functions, and the Pareto optimal set for the problem is generated by systematically varying the weighting parameters for the objective functions. Experimental data are used to validate the final simulation. Several examples are presented to demonstrate the effect of the weighting parameters for the two objective functions on the predicted box-lifting strategies. The results show that the proposed MOO approach improves the simulation results compared to the single objective optimization formulation. Also, the formulation is less sensitive to the weighting coefficient for the stability criterion.

Keywords Lifting · Multiobjective optimization · Effort · Stability · Motion prediction · Predictive dynamics · Optimization

1 Introduction

Human lifting biomechanics is an important issue in many industrial applications [1–3]. Many strategies may be chosen to suit the lifting task depending on the human anthropometry, and weight, position, and shape of the object. Two major strategies have been discussed in the literature: the squat lift and the back lift. However, most biomechanists quantify the

Y. Xiang · J.S. Arora (✉) · S. Rahmatalla · T. Marler · R. Bhatt · K. Abdel-Malek
Virtual Soldier Research (VSR) Program, Center for Computer-Aided Design (CCAD), College of Engineering, The University of Iowa, Iowa City, IA 52242, USA
e-mail: jasbir-arora@uiowa.edu

Y. Xiang
e-mail: yujxiang@engineering.uiowa.edu

lifting strategy based purely on the kinematics of the model, such as the trunk, hip, and knee joint angles.

Kinematics lifting simulation has been discussed in the literature [4]. The basic idea was to quantify the lifting strategy by defining certain indexes. However, the whole-body dynamic lifting motion has not been fully considered in these approaches. The use of dynamic simulation models in investigating the lifting task has recently evolved as a valuable technique that provides insight into the analysis of the lifting motion. Huang et al. [2] developed a multibody dynamics model to generate optimal trajectories of human lifting movements based on optimal control. The muscle activation parameters, instead of joint torques, were treated as inputs. The optimal motion was generated to minimize load on specific joints such as the ankle or knee during the lifting motion and subject to space-time constraints. Arisumi et al. [5] studied the dynamic lifting motion of humanoid robots and considered the instantaneous transfer of load to the robot as an impulsive force. Dysart and Woldstad [3] presented posture prediction for static sagittal plane lifting. Three different objective functions were investigated: dynamic effort, local effort, and stability. Local effort was defined for each joint as torque exerted relative to the strength of the joint. It was concluded that the dynamic effort produced the most accurate lifting motion. Although many performance criteria have been investigated for static or dynamic lifting prediction, use of multiobjective optimization (MOO) for considering the mixed effect of various objective functions has not been studied for the whole-body dynamic lifting problem.

Optimization-based motion prediction has been widely used in biomechanics to synthesize control strategies, analyze muscle forces, predict optimal motion, and so on. However, the performance measure and necessary constraints are critical issues for simulating human motions. Schiehlen [6] gave a review of multibody system dynamics in which optimal design of a mechanical system was discussed, especially the multicriteria optimization approach. Leboeuf et al. [7] compared two performance criteria: the minimum effort cost and the minimum energy cost for predicting human handstand motion. It was concluded that the former tended to generate more natural motion and the latter gave a smoother motion. Bottasso et al. [8] proposed a computational procedure for inferring cost functions that underlie the experimentally observed human strategies.

In the present work, a MOO-based predictive dynamics formulation is developed to simulate spatial dynamic human lifting. Predictive dynamics is defined as an optimization-based method to simulate human motion to determine both kinematics and kinetics of the model [9, 10]. The MOO problem is solved in order to predict the lifting motion and to study the contributions of each performance measure. Two performance measures are investigated: the dynamic effort and stability. Dynamic effort is represented as the time integral of the squares of all the joint torques. Dynamic stability is measured as the summation of distance squares between the zero moment point (ZMP) and the support polygon boundaries during the lifting motion.

In this study, the multibody human system is first described in Sect. 2, and the equations of motion and sensitivities are also detailed. Section 3 covers the details of the proposed optimization formulation for lifting problem. Section 4 presents computational procedures for the MOO problem, and box-lifting simulation results are analyzed in Sect. 5. Finally, concluding remarks are given in Sect. 6.

2 Multibody human system

This section discusses the human modeling and equation of motion for the multibody human system using the recursive Lagrange method.

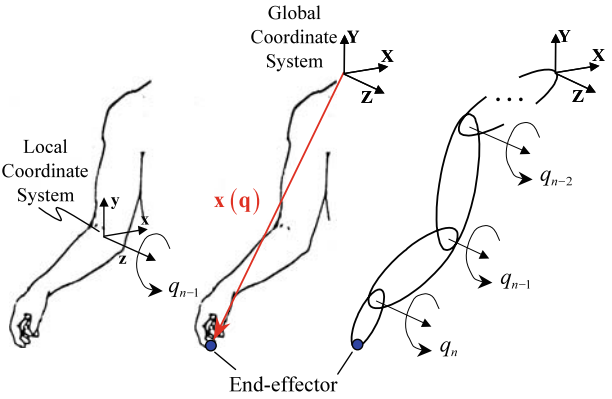

Fig. 1 A kinematic chain of joints

2.1 Human skeletal model

The human skeletal system is highly redundant from a dynamics perspective, meaning there are infinitely many ways to perform a dynamic task. Accordingly, this means there are infinitely many solutions to most inverse dynamics problems involving the human body. However, it is possible to determine a single realistic motion by using optimization.

Simulation of human motion depends largely on how the human skeleton is modeled. We view a skeleton as a series of links with each pair of links connected by one or more revolute joints. Therefore, a complete human body can be modeled as several kinematic chains, as shown in Fig. 1. q_i is a *joint angle* that represents the rotation of a single revolute joint. There is one joint angle for each degree of freedom (DOF). $\mathbf{q} = [q_1, \ldots, q_n]^T \in R^n$ is the vector of joint angles in an n-DOF model and represents a specific posture. Each skeletal joint is modeled using one or more kinematic revolute joints. $\mathbf{x}(\mathbf{q}) \in R^3$ is the position vector in Cartesian space that describes the location of the end-effector with respect to a global coordinate system. For a given set of joint angles $\mathbf{q}$, $\mathbf{x}(\mathbf{q})$ is determined using the Denavit–Hartenberg (DH) method [11]. The DH method uses a series of transformation matrices to translate from the joint space to the Cartesian space.

A three-dimensional digital human skeletal model with 55 DOFs, as shown in Fig. 2, is considered in this work. The model consists of six physical branches and one virtual branch. The physical branches include the right leg, the left leg, the spine, the right arm, the left arm, and the head. Each DOF represents relative rotation/translation of two body segments connected by a revolute/prismatic joint. The virtual branch contains six global DOFs, including three global translations (z_1, z_2, z_3) and three global rotations (z_4, z_5, z_6). This branch is used for moving the model from the origin (o-xyz) of the Cartesian coordinate system to the current pelvic position. The anthropometric data of a 50th percentile male, generated using GEBOD software [12], is used in this study.

2.2 Equations of motion and sensitivities

There are many methods to derive the equation of motion for multibody human dynamics, such as the Euler–Newton method and the Lagrange method. However, in this work, the recursive formulation is used to calculate the kinematics and dynamics for the system because of its computational efficiency. In this process, the forward kinematics propagates the motion from the base point to the end-effectors. In contrast, the backward dynamics transfer the forces from the end-effectors to the base point.

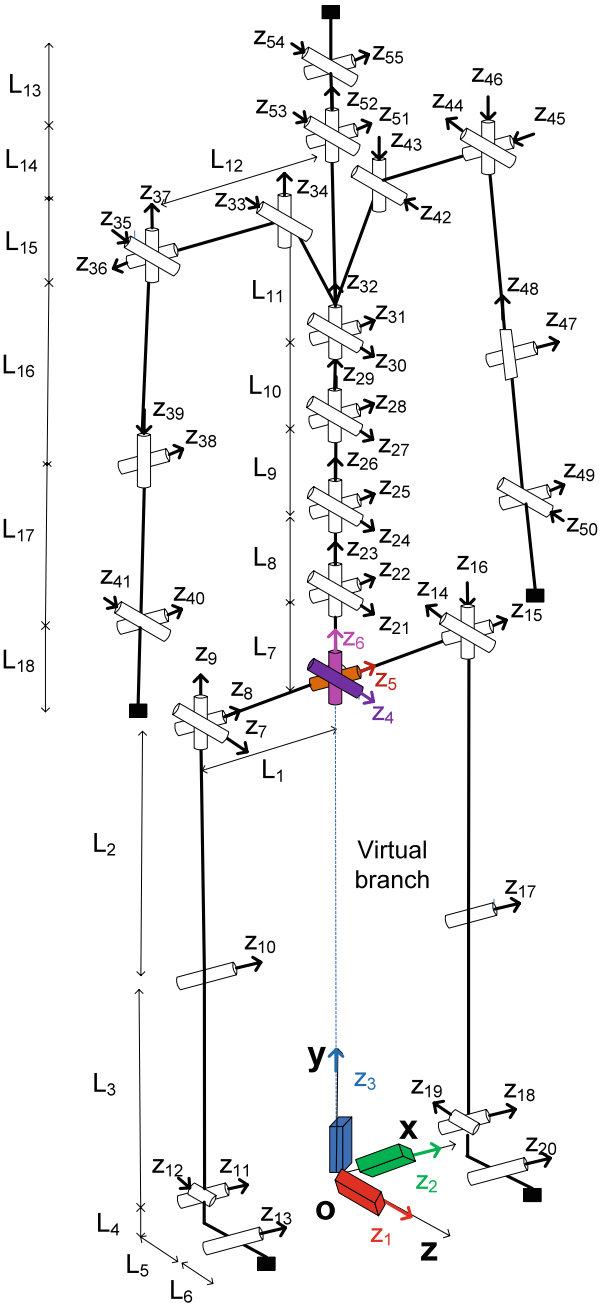

Fig. 2 The 55-DOF digital human model (with global DOFs $z_1, z_2, z_3, z_4, z_5, z_6$), modified from [9]

2.2.1 *Forward recursive kinematics*

In this process, 4×4 matrices $\mathbf{A}_j, \mathbf{B}_j, \mathbf{C}_j$ are defined to represent recursive position, velocity, and acceleration transformation matrices for the jth joint, respectively. Given the link transformation matrix ($\mathbf{T}_j$) and the kinematics state variables for each joint, angular

displacement, velocity, and acceleration (q_j, $\dot{q}_j$, and $\ddot{q}_j$), we have for $j = 1$ to n [13, 14]:

$$\mathbf{A}_j = \mathbf{T}_1\mathbf{T}_2\mathbf{T}_3\cdots\mathbf{T}_j = \mathbf{A}_{j-1}\mathbf{T}_j \tag{1}$$

$$\mathbf{B}_j = \dot{\mathbf{A}}_j = B_{j-1}\mathbf{T}_j + \mathbf{A}_{j-1}\frac{\partial \mathbf{T}_j}{\partial q_j}\dot{q}_j \tag{2}$$

$$\mathbf{C}_j = \dot{\mathbf{B}}_j = \ddot{\mathbf{A}}_j = \mathbf{C}_{j-1}\mathbf{T}_j + 2\mathbf{B}_{j-1}\frac{\partial \mathbf{T}_j}{\partial q_j}\dot{q}_j + \mathbf{A}_{j-1}\frac{\partial^2 \mathbf{T}_j}{\partial q_j^2}\dot{q}_j^2 + \mathbf{A}_{j-1}\frac{\partial \mathbf{T}_j}{\partial q_j}\ddot{q}_j \tag{3}$$

where $\mathbf{A}_0 = \mathbf{1}$ and $\mathbf{B}_0 = \mathbf{C}_0 = \mathbf{0}$. Then the global position, velocity, and acceleration of a point in the Cartesian coordinate system can be calculated using the following formulas:

$$^0\mathbf{r}_j = \mathbf{A}_j\mathbf{r}_j; \qquad ^0\dot{\mathbf{r}}_j = \mathbf{B}_j\mathbf{r}_j; \qquad ^0\ddot{\mathbf{r}}_j = \mathbf{C}_j\mathbf{r}_j \tag{4}$$

where $^0\mathbf{r}_j$ and $\mathbf{r}_j$ are global and local augmented coordinates, respectively. It is noted that the repeated index is not summed in the above equations or the equations that follow.

2.2.2 *Backward recursive dynamics*

Based on forward recursive kinematics, the backward recursion for the dynamic analysis is accomplished by defining a 4×4 transformation matrix $\mathbf{D}_i$ and 4×1 transformation vectors $\mathbf{E}_i$, $\mathbf{F}_i$, and $\mathbf{G}_i$ as follows: given the mass and inertia properties of each link, the external force $\mathbf{f}_k^{\mathbf{T}} = [^k f_x\ ^k f_y\ ^k f_z 0]$ and the moment $\mathbf{h}_k^{\mathbf{T}} = [^k h_x\ ^k h_y\ ^k h_z 0]$ for the link k, defined in the global coordinate system, the joint actuation torques τ_i for $i = n$ to 1 are computed as [13, 14]:

$$\tau_i = \mathrm{tr}\left[\frac{\partial \mathbf{A}_i}{\partial q_i}\mathbf{D}_i\right] - \mathbf{g}^{\mathbf{T}}\frac{\partial \mathbf{A}_i}{\partial q_i}\mathbf{E}_i - \mathbf{f}_k^{\mathbf{T}}\frac{\partial \mathbf{A}_i}{\partial q_i}\mathbf{F}_i - \mathbf{G}_i^{\mathbf{T}}\mathbf{A}_{i-1}\mathbf{z}_0 \tag{5}$$

$$\mathbf{D}_i = \mathbf{I}_i\mathbf{C}_i^{\mathbf{T}} + \mathbf{T}_{i+1}\mathbf{D}_{i+1} \tag{6}$$

$$\mathbf{E}_i = m_i\,^i\mathbf{r}_i + \mathbf{T}_{i+1}\mathbf{E}_{i+1} \tag{7}$$

$$\mathbf{F}_i = {}^k\mathbf{r}_f\delta_{ik} + \mathbf{T}_{i+1}\mathbf{F}_{i+1} \tag{8}$$

$$\mathbf{G}_i = \mathbf{h}_k\delta_{ik} + \mathbf{G}_{i+1} \tag{9}$$

where $\mathbf{D}_{n+1} = \mathbf{0}$ and $\mathbf{E}_{n+1} = \mathbf{F}_{n+1} = \mathbf{G}_{n+1} = \mathbf{0}$; $\mathbf{I}_i$ is the inertia matrix for link i; m_i is the mass of link i; $\mathbf{g}$ is the gravity vector; $^i\mathbf{r}_i$ is the location of center of mass of link i in the local frame i; $^k\mathbf{r}_f$ is the position of the external force in the local frame k; $\mathbf{z}_0 = [0\ 0\ 1\ 0]^{\mathbf{T}}$ for a revolute joint and $\mathbf{z}_0 = [0\ 0\ 0\ 0]^{\mathbf{T}}$ for a prismatic joint; and δ_{ik} is Kronecker delta.

The first term in the torque expression (equation of motion (EOM)) is the inertia and Coriolis torque, the second term is the torque due to gravity load, the third term is the torque due to external force, and the fourth term represents the torque due to the external moment.

2.2.3 *Sensitivity analysis*

Optimization-based motion prediction is a robust methodology to solve trajectory planning for a redundant mechanical system. Such an optimization problem is usually a large-scale nonlinear programming (NLP) problem. Accurate sensitivity is a key factor for efficiently achieving an optimal solution for a gradient-based optimization algorithm such as the sequential quadratic programming (SQP) method.

In this study, the analytical sensitivity equations are implemented for the 3D articulated human model in a recursive way. The computation cost of the recursive formulation is of order $O(n)$, where n is the number of DOFs. The forward kinematics transfers the motion from the origin toward the end-effector along the branch. In contrast, the backward dynamics propagates forces from the end-effector to the origin.

The derivatives, $\frac{\partial \tau_i}{\partial q_k}$, $\frac{\partial \tau_i}{\partial \dot{q}_k}$, $\frac{\partial \tau_i}{\partial \ddot{q}_k}$ ($i = 1$ to n; $k = 1$ to n), can be evaluated for the articulated spatial human mechanical system in a recursive way using the foregoing recursive Lagrangian dynamics formulation as follows:

$$\frac{\partial \tau_i}{\partial q_k} = \begin{cases} \mathrm{tr}\left(\frac{\partial^2 \mathbf{A}_i}{\partial q_i \partial q_k}\mathbf{D}_i + \frac{\partial \mathbf{A}_i}{\partial q_i}\frac{\partial \mathbf{D}_i}{\partial q_k}\right) - \mathbf{g}^{\mathbf{T}}\frac{\partial^2 \mathbf{A}_i}{\partial q_i \partial q_k}\mathbf{E}_i - \mathbf{f}^{\mathbf{T}}\frac{\partial^2 \mathbf{A}_i}{\partial q_i \partial q_k}\mathbf{F}_i - \mathbf{G}_i^{\mathbf{T}}\frac{\partial \mathbf{A}_{i-1}}{\partial q_k}\mathbf{z}_0 & (k \le i) \\ \mathrm{tr}\left(\frac{\partial \mathbf{A}_i}{\partial q_i}\frac{\partial \mathbf{D}_i}{\partial q_k}\right) - \mathbf{g}^{\mathbf{T}}\frac{\partial \mathbf{A}_i}{\partial q_i}\frac{\partial \mathbf{E}_i}{\partial q_k} - \mathbf{f}^{\mathbf{T}}\frac{\partial \mathbf{A}_i}{\partial q_i}\frac{\partial \mathbf{F}_i}{\partial q_k} & (k > i) \end{cases} \tag{10}$$

$$\frac{\partial \tau_i}{\partial \dot{q}_k} = \mathrm{tr}\left(\frac{\partial \mathbf{A}_i}{\partial q_i}\frac{\partial \mathbf{D}_i}{\partial \dot{q}_k}\right) \tag{11}$$

$$\frac{\partial \tau_i}{\partial \ddot{q}_k} = \mathrm{tr}\left(\frac{\partial \mathbf{A}_i}{\partial q_i}\frac{\partial \mathbf{D}_i}{\partial \ddot{q}_k}\right) \tag{12}$$

More details about the derivation of sensitivity equations are provided by Xiang et al. [14].

2.3 Dynamic stability and ground reaction force (GRF)

The dynamic stability condition for the lifting motion is satisfied by forcing the ZMP to stay in the feet support polygon as shown in Fig. 3. The two feet are fixed on the ground with the distance d and orientation angle θ during the lifting motion. ZMP is a well-known bipedal dynamic stability criterion that has been used widely in the literature. It is defined as the point on the ground at which the resultant tangential moments are zero [15].

In this study, an active-passive algorithm is used to calculate ZMP and GRF to obtain the real joint torques for the multibody human system. Details of the algorithm are presented by Xiang et al. [10] and outlined here as follows:

(1) Given state variables $q, \dot{q}, \ddot{q}$ (design variables) for each DOF, the global resultant active forces $(\mathbf{M}^o, \mathbf{F}^o)$ at the origin in the inertial reference frame (o-xyz in Fig. 2) are obtained from equations of motion using inverse dynamics.
(2) After that, the ZMP position is calculated from its definition using the global resultant active forces as follows:

$$y_{\mathrm{zmp}} = 0; \qquad x_{\mathrm{zmp}} = \frac{M_z^o}{F_y^o}; \qquad z_{\mathrm{zmp}} = \frac{-M_x^o}{F_y^o} \tag{13}$$

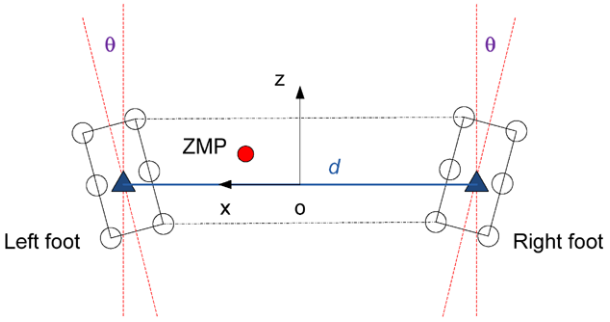

Fig. 3 Feet locations and support region

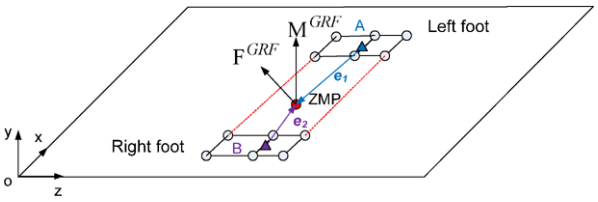

Fig. 4 Partition of the GRF into two feet: e_1 and e_2 are distances between ZMP and feet ball centers

where $\mathbf{M}^o = [M_x^o M_y^o M_z^o]^{\mathbf{T}}$ and $\mathbf{F}^o = [F_x^o F_y^o F_z^o]^{\mathbf{T}}$. In addition, the two feet are assumed on the level ground.

(3) After obtaining the ZMP position, the resultant active forces at ZMP ($\mathbf{M}^{\text{zmp}}$, $\mathbf{F}^{\text{zmp}}$) are computed using the equilibrium condition as follows:

$$\begin{aligned} \mathbf{M}^{\text{zmp}} &= \mathbf{M}^o + \mathbf{F}^o \times {}^o\mathbf{r}_{\text{zmp}} \\ \mathbf{F}^{\text{zmp}} &= \mathbf{F}^o \end{aligned} \tag{14}$$

where ${}^o\mathbf{r}_{\text{zmp}}$ is the ZMP position in the global coordinate system obtained from (13).

(4) Then the value and location of GRF are calculated from the equilibrium between the resultant active forces and passive forces at the ZMP:

$$\begin{aligned} \mathbf{M}^{\text{GRF}} + \mathbf{M}^{\text{zmp}} &= \mathbf{0} \\ \mathbf{F}^{\text{GRF}} + \mathbf{F}^{\text{zmp}} &= \mathbf{0} \\ {}^o\mathbf{r}_{\text{GRF}} - {}^o\mathbf{r}_{\text{zmp}} &= \mathbf{0} \end{aligned} \tag{15}$$

Next, the resultant GRF is partitioned into two feet by using a linear distance relationship between the GRF location and feet centers as shown in Fig. 4.

(5) Finally, all active forces (gravity, inertia and external forces) and passive forces (GRF) are applied to the multibody human system using (5) to obtain the real joint torques that are used in the torque limit constraints and to calculate the dynamic effort objective function.

3 Formulation

3.1 Lifting task

In this work, the lifting task is defined as moving a box from an initial location to a final location. Figure 5 depicts the input parameters for the proposed formulation. In this regard, h_1 is the initial height of the box measured from the ground, d_1 is the initial distance measured from the foot location to the center of the box, h_2 is the final height measured from the ground, d_2 is the final distance, and w is the weight of the box. The initial and final postures and dynamic lifting trajectory are determined by solving a nonlinear optimization problem. The mechanical system is at rest at the initial and final time points.

3.2 Optimization formulation

The lifting motion is predicted by solving a multi-objective optimization problem. In the proposed formulation, the box initial and final locations, feet locations and orientations, and

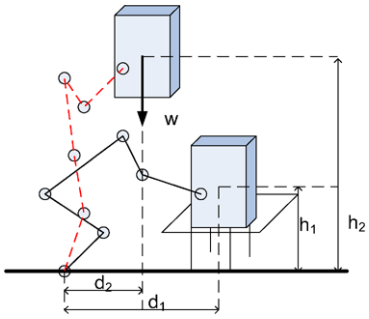

Fig. 5 Input parameters for lifting task

box dimension and weight are given. The total time T for the lifting motion is specified. The initial and final postures are also optimized along with the lifting motion instead of specifying them from the experiments.

3.2.1 Design variables and time discretization

For the optimization problem, the time domain is discretized by using cubic B-spline functions. Thus, a joint profile $q(t)$ is parameterized as follows:

$$q_j(\mathbf{t}, \mathbf{P}) = \sum_{i=1}^{m} N_i(\mathbf{t}) p_i \quad 0 \le t \le T \tag{16}$$

where $N_i(\mathbf{t})$ are the basis functions, $\mathbf{t} = \{t_0, \ldots, t_s\}$ is the knot vector, and $\mathbf{P}_j = \{p_1, \ldots, p_m\}$ is the control points vector. With this representation, the control points become the optimization design variables. In this study, the knot vector is specified and fixed in the optimization process.

The lifting task is formulated as a general nonlinear programming (NLP) problem. To find the optimal control points $\mathbf{P}$ for the lifting motion, a human performance measure, $F(\mathbf{P})$, is minimized subject to physical constraints as follows:

$$\begin{array}{lll} \text{Find:} & \mathbf{P} & \\ \text{To:} & \min & F(\mathbf{P}) \\ \text{Sub.} & h_i = 0, & i = 1, \ldots, m \\ & g_j \le 0, & j = 1, \ldots, k \end{array} \tag{17}$$

where h_i are the equality constraints and g_j are the inequality constraints.

The joint angle profile for each DOF is represented by five control points. Therefore, there are 275 design variables. In addition, the total time duration is discretized into four evenly distributed segments, and five time grid points are used for the entire motion as shown in Fig. 6, where the horizontal scale shows the knot vector. Multiplicity at the ends is used in the knot vector. For B-splines, multiplicity property guarantees that the initial and final joint angle values of a DOF are exactly those corresponding to the initial and final control point values. The time-dependent constraints are imposed not only at the knot points but also between the adjacent knots, so that a smooth motion can be generated.

Since $q, \dot{q}$, and $\ddot{q}$ are functions of $\mathbf{t}$ and $\mathbf{P}$, torque $\tau = \tau(\mathbf{t}, \mathbf{P})$ is an explicit function of the knot vector and control points. Thus, the derivatives of a torque with respect to the control points can be computed using the chain rule as

$$\frac{\partial \tau}{\partial P_i} = \frac{\partial \tau}{\partial q}\frac{\partial q}{\partial P_i} + \frac{\partial \tau}{\partial \dot{q}}\frac{\partial \dot{q}}{\partial P_i} + \frac{\partial \tau}{\partial \ddot{q}}\frac{\partial \ddot{q}}{\partial P_i} \tag{18}$$

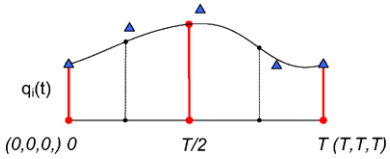

Fig. 6 B-spline discretization of a joint profile

Equations (10)–(12) and (18) are used to calculate accurate gradients for the optimizer to improve the computational efficiency.

3.2.2 Objective functions

For the dynamic lifting motion prediction problem, two performance measures are investigated. The first one is to minimize the dynamic effort, which is defined as the time integral of the squares of all joint torques; the second one is to maximize the stability, which can be transformed to minimize the time integral of the distance squares between ZMP, defined in Sect. 2.3, and foot support boundaries. The weighted sum of the two objective functions is used as the performance measure as follows:

$$F(\mathbf{P}) = w_1 \mathbf{N}\left(\int_{t=0}^{T} \tau(\mathbf{P},t)^{\mathbf{T}} \tau(\mathbf{P},t)\, dt\right) + w_2 \mathbf{N}\left(\int_{t=0}^{T} \left(\sum_{i=1}^{\text{nb}} s(t)_i^2\right) dt\right) \tag{19}$$

where s_i is the distance between ZMP and the ith foot support boundary at time-t; nb is the number of foot support boundaries; w_1 and w_2 are weighting coefficients for the two objective functions ranging from 0 to 1, respectively; and $w_1 + w_2 = 1$. The symbol $\mathbf{N}(\cdot)$ is a normalization operator. A general function-transformation method [16] is used to determine the normalization operator in (19). Details are illustrated in Sect. 4. The effects of different objective functions for the predicted box-lifting strategy are demonstrated in Sect. 5.

3.2.3 Constraints

Two types of constraints are considered for the lifting optimization problem. One type is the time-dependent constraints, which include joint limits, torque limits, ground penetration, dynamic balance, foot locations, vision, hand orientation, and collision avoidance. These constraints are imposed throughout the time interval. The second type is time-independent constraints, which comprise the initial and final box locations and the initial and final static conditions; these constraints are considered only at the starting and ending time points for the lifting motion.

For the lifting task, joint angle limits, torque limits, ground penetration, foot locations, and dynamic balance constraints are detailed by Xiang et al. [10], which simulates a symmetric walking motion using a one-step formulation. The vision, hand orientation, collision avoidance, initial and final box locations, and initial and final static conditions are new constraints for the lifting problem. These new constraints are depicted in Fig. 7 and illustrated as follows.

(1) Vision

The vision constraint is to align the eye vector $\mathbf{r}_{\text{eye}}$ with the vision vector $\mathbf{r}_{\text{vision}}$, which itself is aligned to the box center. The vision vector is defined as a vector from the midpoint of the two eyes to the box center. The eye vector is defined as a vector located at the midpoint of the eyes and normal to the forehead as shown in Fig. 8.

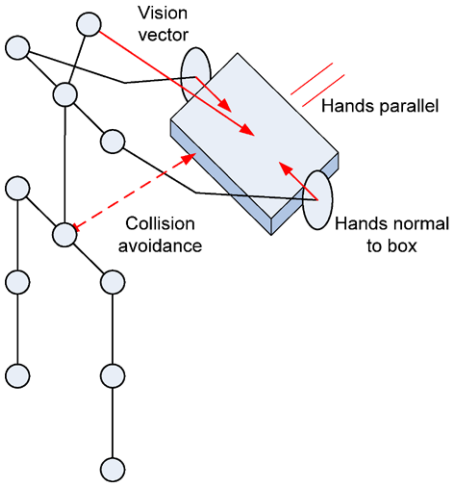

Fig. 7 Hand orientation, vision, and collision-avoidance constraints

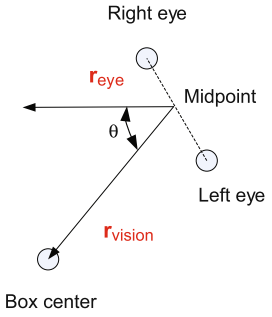

Fig. 8 Vision constraint

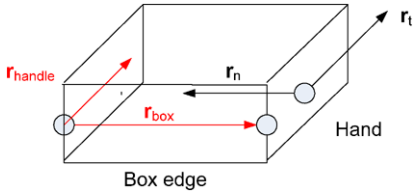

Fig. 9 Hand-orientation constraint

$$\alpha \leq \theta = \arccos\left(\frac{\mathbf{r}_{\text{eye}} \cdot \mathbf{r}_{\text{vision}}}{\|\mathbf{r}_{\text{eye}}\| \|\mathbf{r}_{\text{vision}}\|}\right) \leq \beta \tag{20}$$

where α and β define the vision cone.

(2) Hand distance and orientation

In the lifting process, the hand distance is a constant defined by the box dimension. In addition, the hand orientation is controlled by two vectors: hand normal vector $\mathbf{r}_n$ and hand tangential vector $\mathbf{r}_t$, as depicted in Fig. 9. The orientation constraints are imposed in such a way that the hand normal vector is parallel to the box edge vector $\mathbf{r}_{\text{box}}$ and the hand tangential vector is parallel to the box handle vector $\mathbf{r}_{\text{handle}}$.

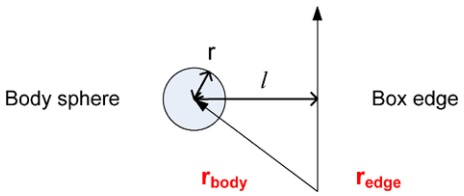

Fig. 10 Collision avoidance constraint between the box and the body

$$\begin{aligned} \mathbf{r}_{\mathrm{n}} \times \mathbf{r}_{\mathrm{box}} &= \mathbf{0}, \\ \mathbf{r}_{\mathrm{t}} \times \mathbf{r}_{\mathrm{handle}} &= \mathbf{0}. \end{aligned} \tag{21}$$

(3) Collision avoidance

The human body is filled with spheres on the ankle, knee, hip, shank, thigh, chest, and neck of various radii to represent the body dimensions. The distances between the box edge and all sphere centers are calculated to impose collision avoidance as shown in Fig. 10. Collision avoidance is considered in the current formulation to prevent penetration of the box in the body.

$$l = \frac{\|\mathbf{r}_{\mathrm{body}} \times \mathbf{r}_{\mathrm{edge}}\|}{\|\mathbf{r}_{\mathrm{edge}}\|} \geq r \tag{22}$$

where r is the radius of the sphere to represent a body segment, and l is the distance between the sphere center and the box surface.

(4) Initial and final hand positions

The hand-contacting positions are specified at the initial and final times for the lifting motion. It is noted that the initial and final postures are determined by the optimization process instead of specifying them from experiments.

$$\begin{aligned} \mathbf{x}(0) &= \tilde{\mathbf{x}}(0), \\ \mathbf{x}(T) &= \tilde{\mathbf{x}}(T), \end{aligned} \tag{23}$$

where $\mathbf{x}$ is the calculated hand position, and $\tilde{\mathbf{x}}$ is the specified hand contacting position.

(5) Initial and final static conditions

The entire body is at rest at the initial and final time points. These conditions are implemented as equality constraints as follows:

$$\begin{aligned} \dot{q}_i(0) &= 0, \\ \dot{q}_i(T) &= 0, \quad i = 1, \ldots, n \end{aligned} \tag{24}$$

where n is the number of degrees of freedom.

4 Computational procedures for MOO using weighted sum approach

A sequential quadratic programming (SQP) algorithm in SNOPT [17] is used to solve the nonlinear optimization problem of lifting motion prediction. To use the algorithm, cost and constraint functions and their gradients need to be calculated. The recursive kinematics and

Table 1 Task parameters for the box lifting

Parameters	
Box weight (Kg)	9.0
Box width (m)	0.525
Box height (m)	0.365
Box depth (m)	0.370
d_1 (m)	0.490
h_1 (m)	0.365
d_2 (m)	0.460
h_2 (m)	1.370
T (s)	1.2

Table 2 Function-comparison matrix

	Dynamic effort F_1 [(N m)^2 s]	Stability F_2 [m^2 s]
Minimize dynamic effort, $\mathbf{q}_1^*$	53 806	0.002690
Minimize stability, $\mathbf{q}_2^*$	117 852	0.001791

dynamics provides accurate gradients to improve the computational efficiency of the optimization algorithm [14, 18]. The adaptive lifting strategies are predicted for box lifting by solving the NLP problem. The data related to the box-lifting task are obtained from an experiment as depicted in Table 1.

4.1 Normalization of objective functions

For MOO, each objective function is normalized using the *upper-lower-bound* transformation approach as follows [16]:

$$F_i^{\mathrm{N}} = \frac{F_i(x) - F_i^{\min}}{F_i^{\max} - F_i^{\min}} \tag{25}$$

where $F_i^{\min}$ represents the minimum value for objective-i and $F_i^{\max}$ represents the maximum value. The general normalization function F_i^{N} has a value between zero and one, depending on the accuracy and the method with which $F_i^{\min}$ and $F_i^{\max}$ are determined. Note that this normalization scheme ensures that the range and magnitudes for the two functions are the same as the range and the magnitudes for the weighting factors.

The optimization problem is solved first using a single objective function without normalization to calculate the $F^{\min}$ and $F^{\max}$ values for each objective function. Table 2 shows the values of the objective functions when each function is minimized independently.

In Table 2, each column represents values for the objective functions F_1 and F_2 calculated at different points. Each row contains values of objective functions calculated at the point $\mathbf{q}_i^*$, which minimizes the ith objective function. The darker boxes indicate the minimum of each function, i.e., the utopia point. The lightly shaded boxes indicate the values of the other function at that optimal point for the function that is optimized. These values are used as the maximum for normalization in (25). As a result, the normalized objective functions are

calculated as follows:

$$F_1^{\mathrm{N}} = \frac{F_1(\mathbf{q}) - 53806}{117852 - 53806}$$
$$F_2^{\mathrm{N}} = \frac{F_2(\mathbf{q}) - 0.001791}{0.002690 - 0.001791} \tag{26}$$

Therefore, the final performance measure for the box-lifting optimization problem is written as

$$F(\mathbf{q}) = w_1 F_1^{\mathrm{N}} + w_2 F_2^{\mathrm{N}} \tag{27}$$

4.2 Articulation of preferences for MOO

When using the weighted sum method for MOO, one either alters the weights systematically in order to approximate the Pareto optimal set and select a final solution (a posteriori articulation for preferences), or one selects a single set of weights a priori that presumably incorporate one's preferences relative to the different objective functions. However, articulating preferences a priori, especially with the weighted sum method, can be a nebulous process. In addition, it is widely recognized that the weighted sum method has inherent deficiencies when it comes to depicting the Pareto optimal set completely. Consequently, we propose a method for selecting weights that minimize the error of the simulation with respect to literature-based lifting determinants. The basic idea is to enumerate the weighting coefficients to minimize the error between the simulation and experiments for some kinematics determinants.

4.2.1 Lifting determinants and error quantification

Based on the literature [19] and experimental observations, six joint angle profiles are chosen as the determinants to define the lifting motion. These determinants correspond to the whole-body motion parameters that have major roles in the task: hip flexion/extension, knee flexion/extension, ankle plantar/dorsiflexion, trunk flexion/extension, shoulder flexion/extension, and elbow flexion/extension.

Errors of these determinants between simulation and experiments are quantitatively studied. In general, the error for the dynamic system at time point t is given as

$$e_i(\mathbf{q}, t) = q_i(t) - \tilde{q}_i(t) \tag{28}$$

where $q_i(t)$ is the simulated ith joint angle profile and $\tilde{q}_i(t)$ is the measured ith joint angle profile at time t. Next, the error throughout the time interval T is given in scalar form using an L_2 norm, which is defined as the following integral:

$$E_i(\mathbf{q}) = \int_0^T \left[e_i(\mathbf{q}, t)\right]^2 dt \tag{29}$$

For box-lifting validation, the total error summation of the six determinants is evaluated as

$$E_{\mathrm{sum}}(\mathbf{q}) = E_{\mathrm{ankle}}(\mathbf{q}) + E_{\mathrm{knee}}(\mathbf{q}) + E_{\mathrm{hip}}(\mathbf{q}) + E_{\mathrm{trunk}}(\mathbf{q}) + E_{\mathrm{shoulder}}(\mathbf{q}) + E_{\mathrm{elbow}}(\mathbf{q}) \tag{30}$$

The total error in (30) is used to quantify accuracy of the predicted lifting motion and to determine weighting coefficients corresponding to each objective function for the multi-objective optimization problem.

4.2.2 *The best combination of preferences*

An enumeration method is used to determine the best coefficients (w_1, w_2), which give minimal error between the simulation and the experimental data. A series of weighted sum problems is solved using a convex combination of objective functions. By varying coefficients w_1 and $w_2 = 1 - w_1$ in (27) systematically, the error sum between the experimental and simulation data for the lifting motion are computed and compared as shown in Fig. 11. In addition, the Pareto optimal curve is plotted in Fig. 12.

In Fig. 11, the smallest error is achieved at $\mathbf{w} = (0.1, 0.9)$ (Point 2 in Fig. 12). Figure 11 suggests that in order to minimize error, effort must be considered to some extent. The simulation with only stability criterion $\mathbf{w} = (0.0, 1.0)$ gives the largest error between the simulation and the experimental data. However, the error for other weighting sets has no significant difference as long as the dynamic effort is considered in the formulation. This indicates that dynamic effort plays an important role in the dynamic box-lifting motion prediction. In addition, it suggests that keeping the ZMP *at the center* of the foot support boundary is not critical.

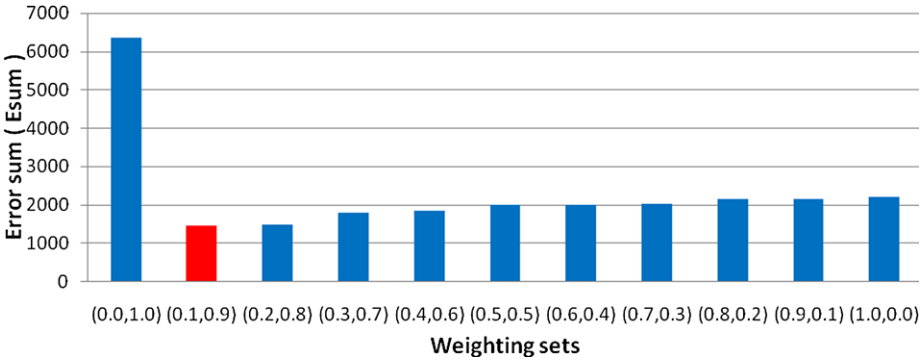

Fig. 11 Error sum between the experimental and simulation determinants for box lifting

Fig. 12 Pareto optimal criterion space

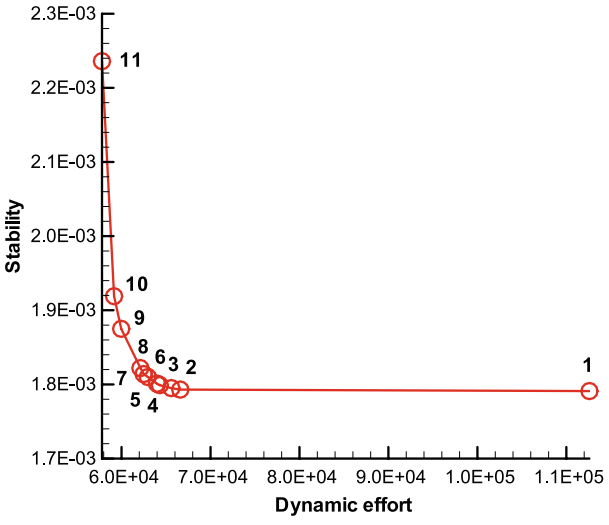

In Fig. 12, it is noted that the Pareto optimal solutions between point 1 $(0.0, 1.0)$ and point 2 $(0.1, 0.9)$ are almost on a horizontal straight line, where the dynamic effort changes substantially but the stability remains at a constant value. This portion of the Pareto optimal curve represents points that are approximately weakly Pareto optimal. Similarly, the optimal solutions between point 9 $(0.8, 0.2)$ and point 11 $(1.0, 0.0)$ are located on a steep vertical line where the stability changes substantially but the dynamic effort does not change much. The optimal solutions between point 2 $(0.1, 0.9)$ and point 8 $(0.7, 0.3)$ are located along a smooth convex curve from which the best solution should be chosen.

If one views the Pareto optimal curve as a trade-off curve, indicating the trade-offs between the two objectives, then there is little advantage to choosing points on flat portions of the Pareto optimal curve. For example, relative to point 2, point 1 represents a substantial increase in effort for just a small improvement in stability. Thus, point 2 is preferred over point 1. A similar conclusion can be drawn for points 9 through 10, relative to point 8. Note that $\mathbf{w} = (0.1, 0.9)$ corresponds to point number 2 in Fig. 12, which is relatively close (but not as close as possible) to the utopia point. The utopia point indicates the point at which both effort and stability have their independent minima. Typically, with a MOO problem, the utopia point is the ideal solution. However, with optimization-based human modeling, the intent is not necessarily to minimize both stability and effort completely. Rather, the intent is to find and minimize that function (performance measure) that governs human behavior most effectively. Minimizing the weighted sum represents one step in the process of determining that governing function.

5 Simulation and validation

Based on the preferences obtained in the previous section, the box lifting is simulated by solving the MOO problem, and the simulation results are validated with the experimental data in this section. The effects of different objective functions are also illustrated. The optimal solution is obtained in 71 seconds on a computer with an Intel(R) dual core 3.16 GHz CPU and 8 GB RAM starting from a feasible solution [10].

5.1 Simulation

The snapshots of simulated lifting motion using stability, dynamic effort, and the weighted sum performance measures are depicted in Fig. 13. The ZMP trajectories for the box-lifting simulations using different performance measures are illustrated in Fig. 14. In addition, GRF and joint torque profiles obtained from the motion prediction using the MOO approach are shown in Figs. 15 and 16, respectively.

It can be seen that the stability criterion predicts a back-lift box-lifting motion in which a large spine flexion occurs without obvious knee bending as shown in Fig. 13a. The predicted lifting motion gives maximum stability, and the ZMP trajectory focuses around the center of the support polygon in Fig. 14a. In contrast, the dynamic effort performance measure predicts a more natural back-lift lifting motion as shown in Fig. 13b. Knee, spine, and shoulder flexions occur simultaneously, and the ZMP trajectory moves in a relatively larger area in the support polygon in Fig. 14b. Finally, the weighted sum performance measure produces a lifting motion that is quite similar to the one predicted using the dynamic effort as the performance measure as seen in Fig. 13c. However, the predicted ZMP trajectory varies in a small area in the support polygon in Fig. 14c. It is evident that the MOO approach shows the combination effects of the two objective functions and also predicts a more natural lifting motion.

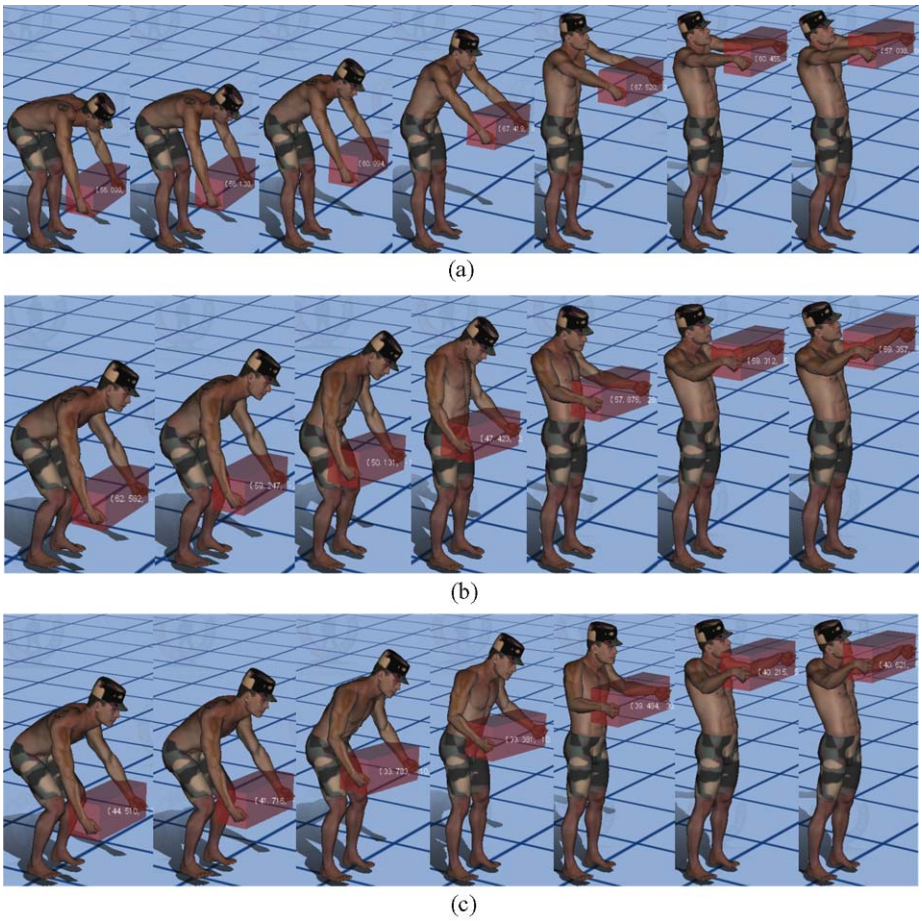

Fig. 13 Snapshots of simulated box lifting motion **a** stability criterion, **b** dynamic effort criterion, **c** weighted sum $w_1 = 0.1$ and $w_2 = 0.9$

The GRF and joint torque profiles for the box-lifting motion are also obtained by solving the optimization problem. The GRFs on both feet are similar in both trends and magnitudes as shown in Fig. 15 (GRF is shown as a fraction of the body weight). In addition, the vertical GRF on each foot takes about half of the body and box weights. The fore-aft GRF has small values for a symmetric box-lifting motion. The predicted joint torques for the right knee, hip, shoulder, and elbow are also similar to the values on the left counterparts as depicted in Fig. 16. This is quite reasonable because the initial and final box locations are symmetric in the sagittal plane so that the predicted lifting motion is also symmetric. However, the torque values on the left and right sides of the skeletal model are not exactly the same. This is expected because of the uneven locations of ZMP where GRF are applied as shown in Fig. 14c.

5.2 Validation

In order to ensure the accuracy of the proposed method, motion capture is used to validate the results experimentally. The lifting motion experimental data were collected from five healthy

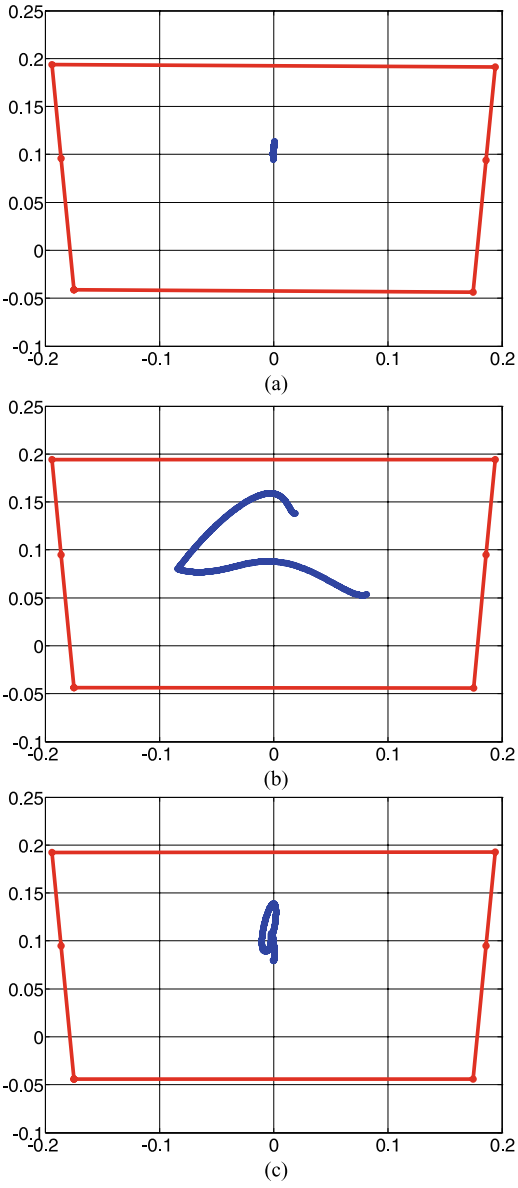

Fig. 14 ZMP and feet support polygon for box lifting with various performance measures **a** stability criterion, **b** dynamic effort criterion, **c** weighted sum $w_1 = 0.1$ and $w_2 = 0.9$

male subjects. The mean height of the subject population was 5′7″ with a mean weight of 143 lbs. The average age of the participants was 34 years. The subjects had no history of musculoskeletal problems and were reasonably fit. Their participation was voluntary, and a written informed consent, as approved by the University of Iowa Institutional Review Board, was obtained prior to testing. During the lifting trials, each subject lifted at a self-selected speed. The experimental data for each subject was also normalized by dividing the cycle time, which is defined as the time duration to lift the object from the initial position to the final position, to directly evaluate the determinants at a percentage of a lifting cycle. For each subject, the time scale was normalized such that the initial posture occurred at time $t = 0$ and

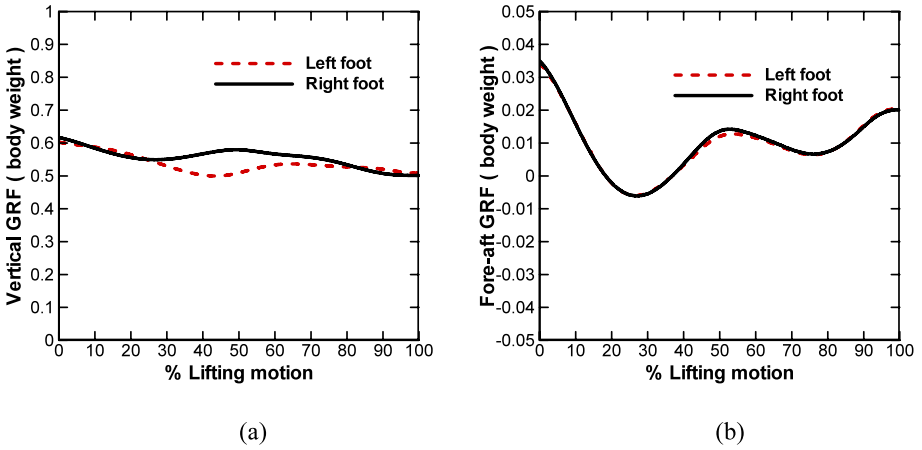

Fig. 15 Ground reaction forces for dynamic box lifting using the weighted sum performance measure **a** vertical GRF, **b** fore-aft GRF

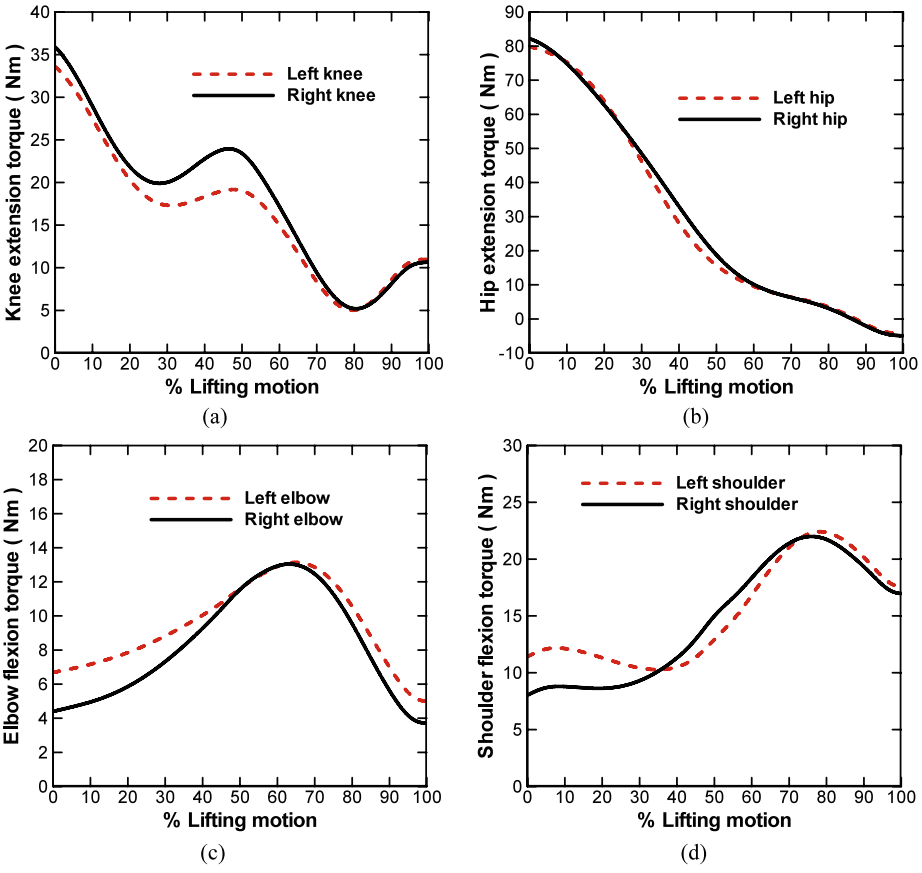

Fig. 16 Joint torque profiles for dynamic box lifting using weight sum performance measure **a** knee extension torque, **b** hip extension torque, **c** elbow flexion torque, **d** shoulder flexion torque

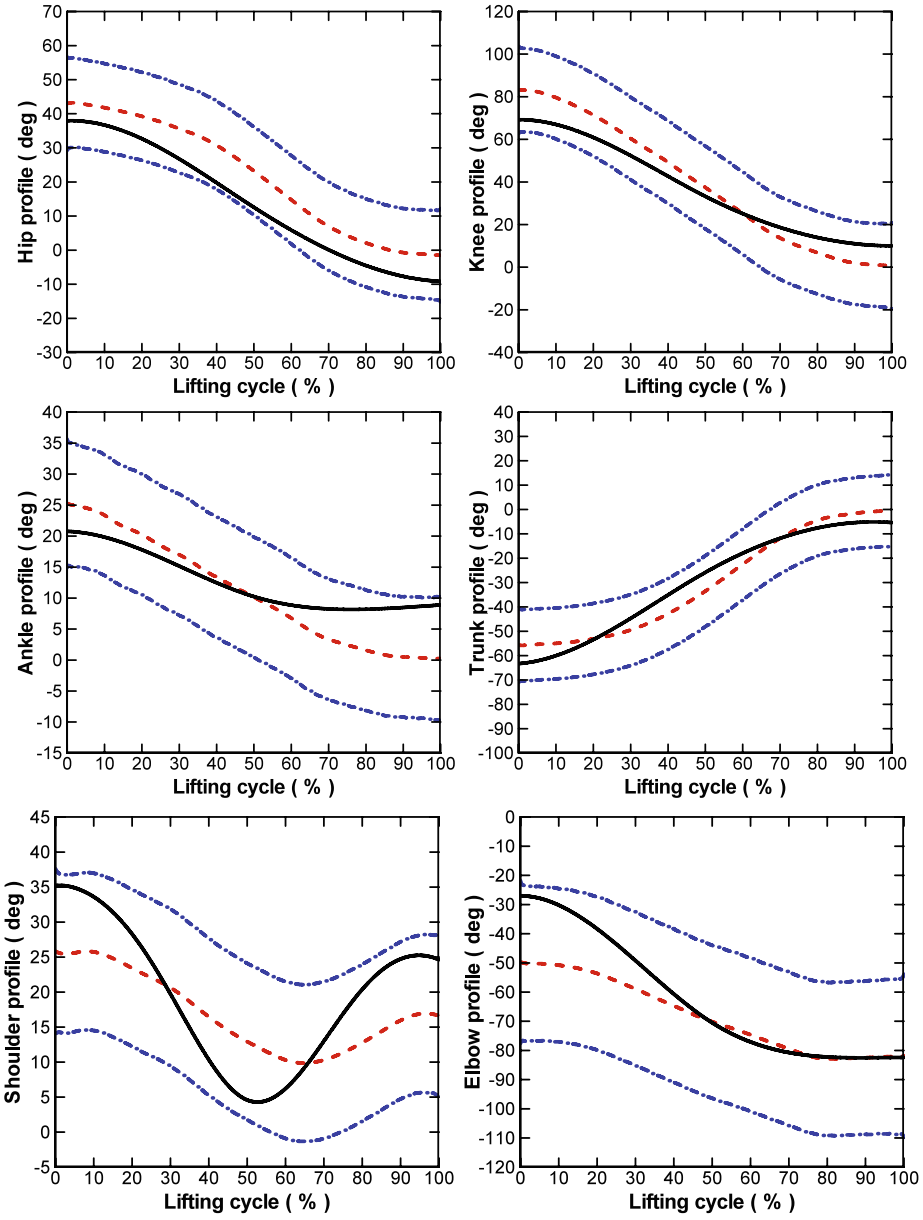

Fig. 17 Comparison of lifting determinants between simulation and experiments

the final posture occurred at time $t = 1$. The lifting motion is validated with experimental determinants as shown in Fig. 17.

Interestingly, the human subjects used similar strategies when conducting the same task. Figure 17 shows the mean and 95% interval of confidence generated from subjects, where the solid curves represent the predicted determinants, the dashed curves are experimental mean value of the determinants, and the dash-dotted curves show 95% confident region of

the statistical means. In general, the predicted lifting motion has shown a good correlation with the experimental data. First, they stay inside the normal region specified by the interval of confidence. Additionally, they show similar trends to those of the mean for the normal subjects. Nevertheless, the dynamic model shows some difficulties predicting the shoulder angle accurately. This may be due in part to the absence of the necessary constraints on the complex shoulder motion in the model and due to the difficulties associated with computing accurate shoulder joint motion from the experimental data. The latter could be contributed to the complex structure of the shoulder joint and the high degree of coupling with the adjacent joints in the human body during the lifting motion. It is noted that the validation for the kinetics data is ongoing and will be reported later.

6 Concluding remarks

In this study, an optimization-based formulation for the lifting motion prediction was presented and some insights on lifting strategy were analyzed. The motion planning was formulated as a large-scale nonlinear programming problem. Joint profiles were discretized using cubic B-splines, and the corresponding control points were treated as unknowns for the optimization problem. Two objective functions were used in the lifting formulation: dynamic effort and stability. An enumeration method was used to determine the best weighting coefficients (w_1, w_2) for the two objectives, which gave minimal error between the simulation and the experimental data. Based on the simulation data, the results have demonstrated the ability of the proposed methodology to choose a realistic human lifting strategy with mixed objective functions and all the constraints.

With the proposed approach, MOO has been used not just to aggregate two functions, but to help determine what governs human behavior during lifting tasks. Using enumeration in conjunction with the weighted sum has allowed us to design an objective function for lifting. In addition, because the components of the weighted sum have physical significance, they provide insight into how and why people act the way they do. Clearly, stability alone is not an adequate driver; it is better suited as a constraint. However, it does play a role in dictating human motion. Minimizing dynamic effort, which depends primarily on joint torque, is a more critical element. Furthermore, this enumeration procedure can be treated automatically by solving a nested optimization problem, in which the MOO lifting problem is solved in the inner loop and the weighting coefficients are determined in the outer loop by minimizing the error sum between the simulation and experiments.

The dynamic lifting motion prediction has a wide variety of applications for biomechanics, ergonomics and human pathology analyses. It is also a robust prototype design tool, e.g., it can be used to study a specific joint injury problem by reducing the corresponding torque limit. Moreover, the lifting strategies can be predicted with different performance measures. It concluded that the dynamic effort performance measure plays important role in lifting motion prediction. The results showed that the proposed MOO approach improved the simulation results; but was less sensitive to the weighting coefficient for the stability criterion.

Acknowledgements This research is partly supported by projects from US Army TACOM, Soldier Systems Center (Natick), and Caterpillar Inc. The authors also gratefully acknowledge Dr. Jingzhou Yang for his helpful comments on the manuscript.

References

1. Chaffin, D.B., Anderson, D.B.J.: Occupational Biomechanics. Wiley, New York (1991)
2. Huang, C., Sheth, P.N., Granata, K.P.: Multibody dynamics integrated with muscle models and space-time constraints for optimization of lifting movements. In: ASME International Design Engineering Technical Conferences. Long Beach, CA, ASME Paper No. DETC2005-85385 (2005)
3. Dysart, M.J., Woldstad, J.C.: Posture prediction for static sagittal-plane lifting. J. Biomech. **29**(10), 1393–1397 (1996)
4. Zhang, X., Nussbaum, M.A., Chaffin, D.B.: Back lift versus leg lift: an index and visualization of dynamic lifting strategies. J. Biomech. **33**(6), 777–782 (2000)
5. Arisumi, H., Chardonnet, J.R., Kheddar, A., Yokoi, K.: Dynamic lifting motion of humanoid robots. In: 2007 IEEE International Conference on Robotics and Automation, Roma, Italy, pp. 2661–2667 (2007)
6. Schiehlen, W.: Multibody system dynamics: roots and perspectives. Multibody Syst. Dyn. **1**, 149–188 (1997)
7. Leboeuf, F., Bessonnet, G., Seguin, P., Lacouture, P.: Energetic versus sthenic optimality criteria for gymnastic movement synthesis. Multibody Syst. Dyn. **16**, 213–236 (2006)
8. Bottasso, C.L., Prilutsky, B.I., Croce, A., Imberti, E., Sartirana, S.: A numerical procedure for inferring from experimental data the optimization cost functions using a multibody model of the neuromusculoskeletal system. Multibody Syst. Dyn. **16**, 123–154 (2006)
9. Xiang, Y., Chung, H.J., Kim, J.H., Bhatt, R., Rahmatalla, S., Yang, J., Marler, T., Arora, J.S., Abdel-Malek, K.: Predictive dynamics: an optimization-based novel approach for human motion simulation. Struct. Multidiscip. Optim. (2009). doi:10.1007/s00158-009-0423-z
10. Xiang, Y., Arora, J.S., Rahmatalla, S., Abdel-Malek, K.: Optimization-based dynamic human walking prediction: one step formulation. Int. J. Numer. Methods Eng. **79**(6), 667–695 (2009)
11. Denavit, J., Hartenberg, R.S.: A kinematic notation for lower-pair mechanisms based on matrices. Trans. ASME J. Appl. Mech. 215–221 (1955)
12. Cheng, H., Obergefell, L., Rizer, A.: Generator of body (GEBOD) Manual, AL/CF-TR-1994-0051. Armstrong Laboratory, Wright-Patterson Air Force Base, OH (1994)
13. Toogood, R.W.: Efficient robot inverse and direct dynamics algorithms using micro-computer based symbolic generation. In: IEEE International Conference on Robotics and Automation, Scottsdale, AZ, pp. 1827–1832 (1989)
14. Xiang, Y., Arora, J.S., Abdel-Malek, K.: Optimization-based motion prediction of mechanical systems: sensitivity analysis. Struct. Multidiscip. Optim. **37**(6), 595–608 (2009)
15. Vukobratović, M., Borovac, B.: Zero-moment point—thirty five years of its life. Int. J. Humanoid Robot. **1**(1), 157–173 (2004)
16. Marler, R.T., Arora, J.S.: Function-transformation methods for multi-objective optimization. Eng. Optim. **37**(6), 551–570 (2005)
17. Gill, P.E., Murray, W., Saunders, M.A.: SNOPT: An SQP algorithm for large-scale constrained optimization. SIAM J. Optim. **12**(4), 979–1006 (2002)
18. Lee, S.H., Kim, J., Park, F.C., Kim, M., Bobrow, J.E.: Newton-type algorithm for dynamics-based robot movement optimization. IEEE Trans. Robot. **21**(4), 657–667 (2005)
19. Authier, M., Lortie, M., Gagnon, M.: Manual handling techniques: Comparing novices and experts. Int. J. Ind. Ergon. **17**(5), 419–429 (1996)